

D. Masih<sup>1</sup>  
Y. Izumi<sup>1</sup>  
K. Aika<sup>1</sup>  
Y. Seida<sup>2</sup>

<sup>1</sup>Interdisciplinary Graduate  
School of Science and  
Engineering, Tokyo Institute of  
Technology, Yokohama, Japan.

<sup>2</sup>Institute of Research and  
Innovation, Takada, Japan.

## Research Article

# Optimization of an Iron Intercalated Montmorillonite Preparation for the Removal of Arsenic at Low Concentrations\*

A series of iron intercalated montmorillonites (Fe-Monts) were prepared using (i) ion exchange of native sodium and calcium ions with iron ions, (ii) base hydrolysis of inserted iron ions in montmorillonite suspension, and (iii) insertion of pre-hydrolyzed iron colloid in montmorillonite. The materials were characterized by X-ray diffraction and gas adsorption-desorption techniques. The basal  $d(001)$ -spacing and BET specific surface area increased after the intercalation of iron species in montmorillonite. Local iron structure studied by X-ray absorption fine structure (XAFS) spectroscopy showed an unsaturation of the Fe...Fe coordination number ( $N$  2.5) of the intercalated iron species as compared to the bulk iron oxyhydroxides ( $N$  6). The Fe-Monts were employed for arsenic removal from aqueous solutions at low concentration (0.2–16 mg/L). Among the Fe-Monts, the one prepared by the hydrolysis of inserted iron ions, was the best in performance. The saturation adsorption amount of the optimized iron-montmorillonite was 4 and 28 times higher for the removal of arsenite and arsenate, respectively, as compared to bulk iron oxyhydroxide (goethite). Compared with bulk iron oxyhydroxide, the Fe-Monts were superior for arsenate uptake and comparable for arsenite. In addition, arsenite adsorbed on the Fe-Monts was found to be oxidized to arsenate based on XAFS spectroscopy.

**Keywords:** Arsenic, Bioremediation, Contaminated water, Environmental protection

*Received:* August 15, 2006; *revised:* November 16, 2006; *accepted:* November 24, 2006

**DOI:** 10.1002/elsc.200620171

## 1 Introduction

Arsenic contamination of drinking water resources is a major environmental problem in many countries of the world [1, 2]. Both natural and anthropogenic sources have increased arsenic levels of water. Depending upon environmental conditions, arsenic exists in water as arsenite ( $\text{As}^{\text{III}}$ ) and arsenate ( $\text{As}^{\text{V}}$ ) oxyanions or neutral species. The mobility and bioavailability of arsenic highly depends upon the particular species. In particular, arsenite is the most toxic and mobile among all the

common species of arsenic [3]. Due to high health hazards, especially carcinogenic risks from the consumption of arsenic contaminated water, the maximum contaminant level has been reduced from 50  $\mu\text{g/L}$  to 10  $\mu\text{g/L}$  [1, 2, 4]. Adsorption is a simple and economical method for the removal of arsenic from aqueous solutions. However, to cope with new regulations and provide safe drinking water, effective adsorbent materials are required, especially for the removal of arsenite from low concentration solutions.

The affinity of arsenic for iron-based materials is well known [5–9]. However, by using bulk iron oxyhydroxides (e.g., goethite), the removal of arsenite is difficult without prior oxidation [10]. Iron dissolution from soil and its co-precipitation with arsenic is important to control its fate in the environment [11]. In this study, an iron-based adsorbent was chosen and its affinity for arsenic was investigated by preparing different kinds of iron species. Sodium-montmorillonite (Na-Mont), a clay mineral of the smectite group having a three-layered sheet structure, was used as a substrate material to host iron species. Intercalation behavior of montmorillonite is well known [12–15].

**Correspondence:** Y. Izumi (e-mail: izumi.y.ac@m.titech.ac.jp), Interdisciplinary Graduate School of Science and Engineering, Tokyo Institute of Technology, Nagatsuta 4259-G1-16, Midori-ku, Yokohama 226-8502, Japan.

[\*] Based on a lecture presented at the First International Conference on Environmental Science and Technology (ICEST), New Orleans, LA, USA, January 23–26, 2005.

X-ray absorption fine structure (XAFS) spectroscopy is a state-of-the-art technique for the local structure studies [16]. In this paper, XAFS was chosen as a probe for the studies of the molecular level of adsorbent and adsorbate species to gain an understating of the arsenic removal mechanism and to make modifications in the adsorbent material, in order to satisfy modern environmental regulations. Redox behavior of adsorbed arsenic species was monitored by XAFS combined with high-energy-resolution fluorescence spectrometry. Speciation of arsenic at low concentrations (0.13–0.48 wt %) adsorbed on iron species was performed successfully. The high signal/background ratio enabled by this combined technology has been used to monitor low concentrations of environmental contaminants in the presence of other heavy metals [17, 18].

This study describes the preparation of different kinds of iron species intercalated montmorillonites, and the behavior of their physicochemical properties with different iron loadings. The arsenic removal capacity and efficiency of Fe-Monts prepared by different routes are discussed in detail. The arsenic adsorption activity of intercalated iron species is compared with that of bulk iron oxyhydroxides. The importance of intercalated iron species for the oxidative adsorption of most toxic and highly mobile arsenite species is explained.

## 2 Materials and Methods

### Preparation of Iron-Montmorillonites

Iron-montmorillonites (Fe-Monts) were prepared by three routes outlined in Fig. 1. Na-montmorillonite (Kunipia F; 99 % purity) was used as received from Kunimine Industries. The particle size of Na-Mont was in the range of 0.1–1.0  $\mu\text{m}$  and the cation exchange capacity was 115 meq/100 g. The substrate material also had a 2.21 wt % of  $\text{Fe}_2\text{O}_3$  from the substitutions of some aluminum sites in the central layer of the montmorillonite sheet. The iron present in the pristine montmorillonite was essentially buried between the silicon layers. Aqueous solutions of 0.43 M  $\text{Fe}(\text{NO}_3)_3$  (Wako) and 0.75 M NaOH (Wako) were used in all the preparations. All the Fe-Monts were prepared at 290 K using 0.5 wt % aqueous suspension of Na-Mont.

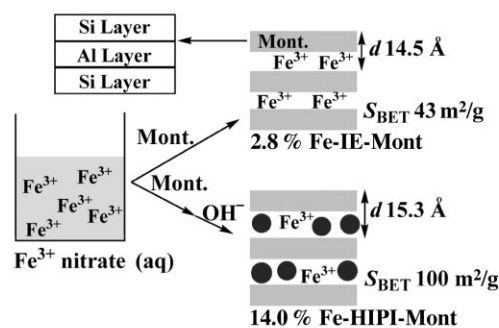
### Ion Exchange (IE)

For the ion exchange reaction, 0.5 mmol of  $\text{Fe}(\text{NO}_3)_3$  was added dropwise into a 0.5 wt % aqueous suspension of Na-Mont (1.0 g) and kept stirring for 12 h. The maximum amount of iron exchanged with the sodium and calcium sites of montmorillonite corresponded to 2.8 wt % on a dry mass basis. If more than 0.5 mmol of  $\text{Fe}(\text{NO}_3)_3$  was introduced to 1.0 g of Na-Mont suspension, the excessive iron was eluted out.

### Hydrolysis of Inserted Positive Ions (HIPI)

An excessive amount of iron ions (> ion exchange capacity) was introduced to a Na-Mont suspension. The inserted positive ions were stabilized by base hydrolysis with a 0.75 M

### (A) Ion Exchange (IE), and Hydrolysis of Inserted Positive Ions (HIPI)



### (B) Insertion of Pre-hydrolyzed Iron (HPI)

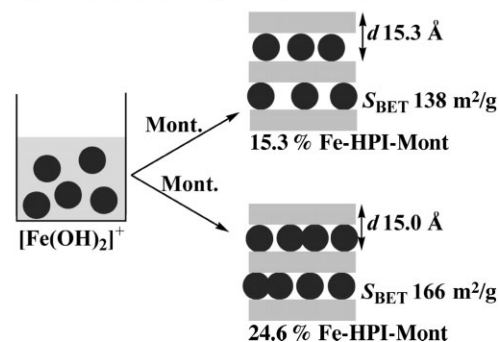


**Figure 1.** Schematic diagram for the preparation of iron-montmorillonites.

NaOH aqueous solution. The OH:Fe molar ratio was a key factor for the successful intercalation of iron species, and the optimized ratio was 2. A series of iron-montmorillonites were prepared using the post-hydrolysis of different amounts of inserted positive ions. For the maximum iron loaded 14.0 % Fe-HIPI-Mont, 3.0 mmol of  $\text{Fe}(\text{NO}_3)_3$  was mixed with 0.5 wt % aqueous suspension of Na-Mont (1.0 g). The amount of iron ions added into montmorillonite suspension was 6 times higher than the exchangeable amount required against the native ions. The mixture was stirred at 290 K for 2 h, and then 6.0 mmol of NaOH was added dropwise. The final reaction mixture was kept on stirring for 12 h.

### Insertion of Pre-Hydrolyzed Iron (IPI)

This method is similar to a previously reported method [14]. In this case, instead of growing iron species in the montmorillonite suspension, pre-hydrolyzed iron species were inserted in the montmorillonite. At first, a precursor colloid of 0.20 M  $[\text{Fe}(\text{OH})_2]^+$  was prepared by mixing  $\text{Fe}(\text{NO}_3)_3$  and NaOH. The molar ratio of base to metal was kept at 2, and the mixing was carried out at 290 K. The colloidal  $[\text{Fe}(\text{OH})_2]^+$  was added to a 0.5 wt % aqueous suspension of the Na-Mont, and stirred for 12 h. A series of Fe-IPI-Monts were prepared with iron loadings ranging from 2.0–27 wt %. By this route, the maxi-

imum amount of iron loaded in the montmorillonite was 27 wt %.

For all the preparations, the solid and liquid phases were separated by filtration. The obtained mass was washed with Millipore water until the pH of the filtrate approached 7. The final product was dried at 313 K for 72 h.

#### X-ray Diffraction and N<sub>2</sub> Adsorption-Desorption Measurements

X-ray diffraction (XRD) patterns of powdered samples were recorded on a Multiflex-S diffractometer (Rigaku) using Cu *K* $\alpha$  radiation. The patterns were measured in the 2-theta range of 2–60 degrees. The gas adsorption-desorption isotherms were measured on BELSORP 28SA and Belsorp-mini (Bell Japan). The isotherms were measured at 77 K using N<sub>2</sub> as an adsorbate. Before recording the isotherms, the samples were outgassed by evacuation at 423 K or by heating at the same temperature for 2 h under N<sub>2</sub> flow. The specific surface area of adsorbents was calculated using the Brunauer-Emmett-Teller (BET) method. Pore size distribution and pore volume were determined from the desorption branch of isotherms using the Dollimore-Heal (DH)-plot method.

#### Arsenic Adsorption Tests

The arsenic adsorption tests were performed in a batch set-up and at 290 K. In a 30 mL capacity polypropylene tube, 50 mg of adsorbent was immersed in 20 mL of 0.2–16 mg/L test solution of arsenite (pH 5.5–6.5) and arsenate (pH 5.7–6.7). The mixture was shaken on a reciprocating shaker at 130 rpm for 12 h. For the adsorption test, an arsenite stock solution (1000 mg/L) was prepared by dissolving As<sub>2</sub>O<sub>3</sub> (Wako) in a minimum amount of basic aqueous solution and the final pH was brought to 7 by the addition of HCl solution [5]. Arsenate stock solution was prepared from water soluble KH<sub>2</sub>AsO<sub>4</sub> (Aldrich). The aqueous phase arsenic concentration was determined by inductively coupled plasma-optical emission spectroscopy (ICP-OES), using Vista-Pro of Seiko-Varian Instruments.

#### Iron K-edge XAFS Measurements

For XAFS measurements, the Fe-Monts were transferred into a Pyrex glass XAFS cell and evacuated at 290 K. Iron K-edge XAFS spectra were measured at the beamline 10B of KEK-PF. A channel-cut Si(311) double crystal monochromator set was used. The measurements were carried out in a transmission mode at 290 K. N<sub>2</sub> and a mixture of N<sub>2</sub>/Ar (85 %/15 %) was used, respectively, in the ionization chambers measuring the *I*<sub>0</sub> (incident) and *I*<sub>t</sub> (transmitted) signal counts. The absorption-edge energy of 4  $\mu$ m iron metal foil was calibrated to 7111.2 eV [19].

#### Arsenic *a* Emission Spectra and K-edge XAFS Measurements

20 mm diameter disks were prepared for the arsenic adsorbed on the Fe-Monts, and the arsenic reference compounds

(Arsenic metal powder, As<sup>III</sup><sub>2</sub>O<sub>3</sub> and KH<sub>2</sub>As<sup>V</sup>O<sub>4</sub>) setting the arsenic K-edge absorption jump value to 1.0. The arsenic K-edge XAFS spectra were measured at an undulator beamline 10XU of SPring-8 (Japan) by utilizing a Rowland-type high-energy-resolution fluorescence spectrometer. A Si(111) double crystal monochromator set was used. In order to suppress higher harmonics, a rhodium-coated double crystal mirror set was inserted at 3.0 mrad into the path of the incident X-ray beam. The secondary spectrometer selectively counts the fluorescence X-rays emitted from the sample over a small energy band (0.3–1.3 eV) and thus enables the measurement of the XAFS spectra with a high-energy resolution [18].

The arsenic *K* $\alpha$ <sub>1</sub> emission peak was measured for each arsenic adsorbed Fe-Mont sample. Then the fluorescence spectrometer was tuned to the peak top of the emission line, and the XAFS spectra were measured by means of this high-energy-resolution detector. All the measurements were carried out at 290 K. A mixture of 15 % Ar and N<sub>2</sub> was flown into the *I*<sub>0</sub> and *I*<sub>t</sub> signal counting ionization chambers. The arsenic absorption K-edge energy was calibrated to 11865.0 eV [19].

The XAFS data were analyzed by using the XDAP (XAFS Services International) programme. For the iron EXAFS analysis, empirical parameters for Fe-O and Fe-Fe bond distances were extracted from the EXAFS spectrum of  $\alpha$ -Fe<sub>2</sub>O<sub>3</sub>. The bond distances and coordination numbers were based on the crystal structure data for  $\alpha$ -Fe<sub>2</sub>O<sub>3</sub> [20, 21]. The values of  $\sigma^2$  are presented as relative ( $\Delta\sigma^2$ ) to those of the corresponding model parameters. The goodness of the fit was given as required by the Committee for Standards and Criteria in X-ray Absorption Spectroscopy.

## 3 Results and Discussion

### 3.1 Basal Spacing with Iron Loading of Montmorillonite

Basal spacing along the (001) direction (*d*-spacing) for the substrate material Na-Mont was 12.2 Å as shown by the low-angle XRD pattern (see Fig. 2). After interaction of montmorillonite particles with iron species >94 % of sodium ions were replaced. The sodium contents of the solutions of the Fe-Monts were determined by ICP-OES. The loss of sodium ions from montmorillonite confirmed a successful intercalation of the iron species.

The low-angle XRD patterns showed that the ordered structure of montmorillonite was retained after iron intercalations (see Fig. 2). For a 2.8 % Fe-IE-Mont, prepared by the ion exchange route, the *d*-spacing increased from 12.2 Å to 14.5 Å (see Tab. 1), which indicated the replacement of native ions with comparatively larger and more hydrated iron species. In this study, sodium and calcium ions of substrate material were completely exchanged with iron ions. One previous study reported a decrease in the *d*-spacing when the introduced iron ions were less than the exchangeable ions in the pristine material [22].

Maximum basal spacing of 15.3 Å was observed for the 14.0 % Fe-HIPI-Mont (see Tab. 1). In the HIPI route, a base

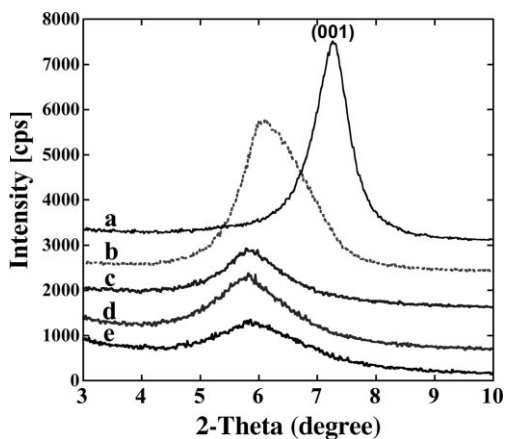


**Figure 2.** Low-angle XRD pattern of the substrate material Na-montmorillonite (a); 2.8 % Fe-IE-Mont (b); 14.0 % Fe-HIPI-Mont (c); 15.3 % Fe-IPI-Mont (d); and 24.6 % Fe-IPI-Mont (e).

hydrolysis of excessive iron ions was performed in the montmorillonite suspension. A successful intercalation was observed for the partially hydrolyzed (base to metal ratio of 2) iron species. On the other hand, for the base to metal ratio of 3, the iron species were mostly precipitated outside of montmorillonite. This argument was supported by the fact that the increase in *d*-spacing was small (12.7 Å) when the base to metal ratios were 3. In the series of Fe-HIPI-Monts, the basal spacing was increasing with the iron loading. In comparison to the Fe-Mont prepared by ion exchange, for the same iron (2.8 wt %) amount intercalated by the HIPI route, the *d*-spacing was 1.8 Å smaller. The reason for the larger basal spacing obtained for the 2.8 % Fe-IE-Mont as compared to the 2.8 % Fe-HIPI-Mont was because of the high amount of water of hydration required for iron but not for the partially hydrolyzed iron species.

The *d*-spacing for the 15.3 % Fe-IPI-Mont (15.3 Å) prepared by insertion of pre-hydrolyzed iron colloid was similar to that of the 14.0 % Fe-HIPI-Mont. When the intercalated iron amount was 24.6 wt %, a decrease in basal spacing was shown by the XRD pattern (see Tab. 1 and Fig. 2). This behavior was in accordance with other studies reporting the relation of metal loading and *d*-spacing of smectite clay [23]. When excessive iron colloid was introduced into the montmorillonite suspension, the maximum amount of iron retained in the material was 27 wt %, however, the ordered structure of iron-montmorillonite was severely damaged, as the (001) peak almost disappeared in the XRD pattern (data not shown). In the case of the Fe-IPI-Monts with different iron loadings, the *d*-spacing was increasing with iron loading up to 15.3 wt %. Any further increase in iron gave the same *d*-spacing (15.3 Å) or a shift towards a smaller value, as shown in Fig. 2 for the 24.6 % Fe-IPI-Mont (15.0 Å). This behavior was similar to the Zr-exchanged pillared clay [23].

For the iron intercalated montmorillonites prepared by the HIPI and IPI routes, the maximum iron loading was 14.0 and 27 wt %, respectively. The *d*-spacing values of the 14.0 % Fe-HIPI-Mont and the 15.3 % Fe-IPI-Mont were the same. Based on the thickness of the montmorillonite sheet, i.e. 9.3 Å [24], the size of the intercalated iron species should be around 6 Å along the (001) direction. For the 14.0 % Fe-HIPI-Mont, some of the introduced iron ions were occupying the point charges on the silicon layer and other partially hydrolyzed species were balancing the overall negative charge on the montmorillonite sheets. Therefore, the intercalated iron species prepared via the HIPI route should be relatively small. Furthermore, the dispersion of iron species intercalated in the montmorillonite, and the Fe···Fe coordinative unsaturation should exceed that of the iron species intercalated by the IPI route.

**Table 1.** Basic physicochemical data of Na-montmorillonite, iron-montmorillonites and bulk iron oxyhydroxides.

Adsorbent	Fe [wt %]		<i>d</i> -spacing [Å]	<i>S</i> <sub>BET</sub> [m <sup>2</sup> /g]	Pore size [Å]	Pore volume [mm <sup>3</sup> /g]
	Intercalated	Total				
Na-montmorillonite	n.a.	1.5	12.2	26	39	33
2.8 % Fe-IE-Mont	2.8	4.3	14.5	43	41	44
14.0 % Fe-HIPI-Mont	14.0	15.3	15.3	100	41	67
15.3 % Fe-IPI-Mont	15.3	16.5	15.3	138	41	93
24.6 % Fe-IPI-Mont	24.6	25.7	15.0	166	41	92
<i>α</i> -FeO(OH)	n.a.	62.8	n.a.	16	n.a.	n.a.
<i>α</i> -FeO(OH) [6]	n.a.	62.8	n.a.	39	n.a.	n.a.
<i>α</i> -FeO(OH) [14]	n.a.	62.8	n.a.	54	n.a.	n.a.

n.a.: not applicable

### 3.2 BET Specific Surface Area and Porosity of Adsorbent Materials

The BET specific surface area ( $S_{\text{BET}}$ ) of the Na-Mont (26 m<sup>2</sup>/g) was in good agreement with the given value (25 m<sup>2</sup>/g). The adsorption-desorption isotherms shown in Fig. 3 A were similar to Type-IIb of IUPAC classification [25]. With the intercalation of the ion exchanged iron (2.8 wt %) species,  $S_{\text{BET}}$  increased to 43 m<sup>2</sup>/g. Furthermore, for the 14.0 % Fe-HIPI-Mont an about four times rise in  $S_{\text{BET}}$  (100 m<sup>2</sup>/g) was observed (see Tab. 1). For the Fe-HIPI-Monts, a linear increase in  $S_{\text{BET}}$  was observed with the increase of an intercalated iron amount. Similarly, the Fe-IPI-Monts also showed a linear increase in  $S_{\text{BET}}$  with the iron loading. A maximum  $S_{\text{BET}}$  of 211 m<sup>2</sup>/g was found for the 27 wt % iron intercalated montmorillonite prepared via the IPI route.

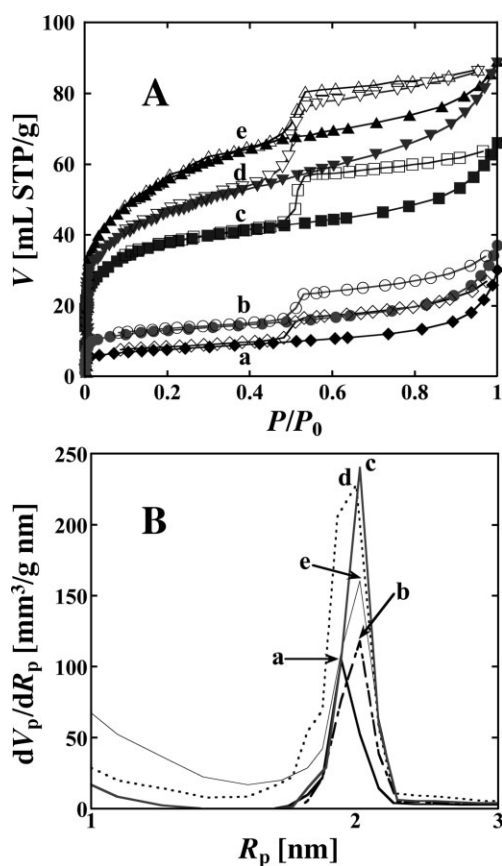


**Figure 3.** (A) N<sub>2</sub> adsorption (solid points)-desorption (hollow points) isotherms for the Na-montmorillonite (a); 2.8 % Fe-IE-Mont (b); 14.0 % Fe-HIPI-Mont (c); 15.3 % Fe-IPI-Mont (d), and 24.6%Fe-IPI-Mont (e).

(B) The corresponding DH-plots from the desorption branch show the pore size distribution.

The pore size distribution and pore volume were calculated by the DH-plot method. A homogeneous distribution with meso-sized (20–500 Å) pores was observed for the adsorbent materials (see Fig. 3 B). Na-Mont had an average pore diameter of 39 Å, which increased to 41 Å after the intercalation of

iron species (see Tab. 1). Pores larger than 41 Å were not observed in any of the Fe-Monts. Basically, the pores in the montmorillonites were slit shaped openings as depicted by the type of the adsorption-desorption isotherms and the characteristic hysteresis loops. The Na-Mont and the 2.8 % Fe-IE-Mont had essentially no micropores (< 20 Å), however, the Fe-HIPI and IPI-Monts showed a peak feature extending below an  $R_p$  (pore radius) of 1 nm as demonstrated in Fig. 3 B. This intrusion gave an indication for the presence of micropores, and it was increasing with iron loading. For the 15.3 % Fe-IPI-Mont,  $S_{\text{BET}}$  was lower than that of the 24.6 % Fe-IPI-Mont, but the pore volume was higher, i.e. 93 mm<sup>3</sup>/g (see Tab. 1). The substantial increase of micropores with iron loading was responsible for the maximum  $S_{\text{BET}}$  value of the 27 % Fe-IPI-Mont.

### 3.3 Arsenic Adsorption Capacity and the Efficiency of Iron-Montmorillonites

The arsenic adsorption isotherms for iron-montmorillonites and bulk iron oxyhydroxide are presented in Fig. 4. The con-

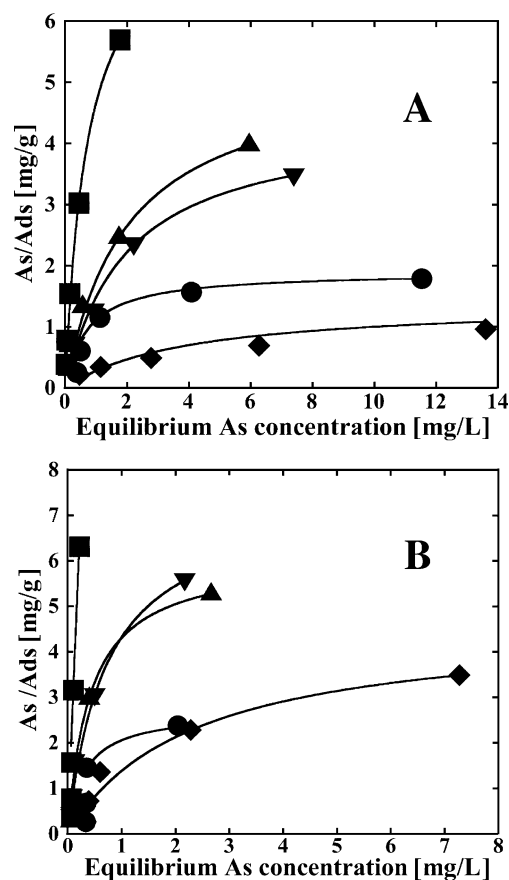


**Figure 4.** Adsorbent weight basis (A) arsenite and (B) arsenate adsorption isotherms for the 2.8 % Fe-IE-Mont (filled diamonds), 14.0 % Fe-HIPI-Mont (filled squares), 15.3 % Fe-IPI-Mont (filled inverted-triangles), 24.6 % Fe-IPI-Mont (filled triangles), and bulk iron oxyhydroxide (goethites) with an  $S_{\text{BET}}$  of 16 m<sup>2</sup>/g (filled circles).

centration range of the arsenic test solutions was chosen as a plausible limit under environmental conditions. The adsorption data fit well with the Langmuir-type equation. Under the experimental conditions, the adsorption of arsenic on the untreated Na-Mont was negligible (see Tab. 2). However, under different conditions, some adsorption of arsenate was observed on montmorillonite [26]. In this study, after the replacement of inactive native sodium ions of montmorillonite with iron, the modified materials became highly active for arsenic removal.

The arsenite saturated adsorption capacity ( $a$ ) of the 2.8 % Fe-IE-Mont was comparable with that of the bulk iron oxyhydroxide ( $\alpha$ -FeO(OH); goethite), and for arsenate, it was higher (see Tab. 2) even though the iron content of  $\alpha$ -FeO(OH) was >14 times of that of the 2.8 % Fe-IE-Mont. In comparison to  $\alpha$ -FeO(OH), the adsorption equilibrium constant ( $K$ ) values of the 2.8 % Fe-IE-Mont were similar for arsenite adsorption, but low in the case of arsenate (see Tab. 2). The arsenic adsorption isotherms plotted on an iron weight basis showed that the 2.8 % Fe-IE-Mont was not only superior to that of the  $\alpha$ -FeO(OH) used in this study, but also to the high  $S_{\text{BET}}$   $\alpha$ -FeO(OH) (39 and 54 m<sup>2</sup>/g) used in other studies [6, 14] (see Tab. 2). Furthermore, the arsenite  $K$  value of the 2.8 % Fe-IE-Mont was higher as compared to the Fe-IPI-Monts. The overall adsorption results showed the presence of a large number of active iron sites in the 2.8 % Fe-IE-Mont, however, the intercalated iron amount could not be increased by more than 2.8 wt % (maximum exchangeable limit) through the ion exchange route.

In addition, the base hydrolysis of the inserted positive ions in the montmorillonite suspension was carried out to stabilize the higher (> 2.8 wt %) iron amount and to increase the number of active sites for arsenic removal. This post-mixing base hydrolysis of excessive iron ions in the montmorillonite allowed for a retention of a 5 times higher iron amount as obtained in the 14.0 % Fe-HIPI-Mont. From the series of the Fe-HIPI-Monts, the adsorbent with a maximum iron loading (14.0 wt %),  $d$ -spacing and  $S_{\text{BET}}$  was chosen for the arsenic adsorption studies. Both the arsenite and arsenate adsorption

capacities of the 14.0 % Fe-HIPI-Mont were maximal among all the adsorbents employed in this study (see Tab. 2). The  $a$  values of arsenite and arsenate adsorption were found to be 4 and 28 times of that of the  $\alpha$ -FeO(OH) applied under the same experimental conditions. A large value for the arsenite adsorption equilibrium constant showed its superiority for low concentration solutions (< 310  $\mu\text{g/L}$ ). In comparison to the Fe-IPI-Mont with a comparable iron content (15.3 wt %) and basal spacing, the adsorption capacities were 1.8 and 10.2 times higher for arsenite and arsenate, respectively (see Tab. 2 and Fig. 4).

The Fe-IPI-Monts were prepared with iron loadings in the range of 2.0–27 wt %. The Fe-Monts with 15.3 and 24.6 wt % iron contents were selected because of the optimum  $d$ -spacing and comparably maximum iron loadings. A saturated arsenic adsorption amount was reached at a maximum for iron/arsenite and arsenate adsorptions of 24.6 wt % and 15.3 wt %, respectively (see Tab. 2 and Fig. 4). Therefore, the arsenic adsorption was not increasing with the increase of the iron amount loaded in the montmorillonite. On the other side, it was a function of the number of the active iron sites present in the adsorbent material. Among all the Fe-Monts, the  $K$  values of the Fe-IPI-Monts were high for the arsenate adsorption, but the saturated arsenic adsorption capacities were significantly lower than those of the 14.0 % Fe-HIPI-Mont (see Tab. 2).

Iron-montmorillonites were superior to bulk iron oxyhydroxides, even though the Fe-Monts have had low iron contents. For the Fe-Monts, the As/Fe molar ratios for both the arsenite and arsenate cases were higher than that of the bulk iron oxyhydroxides (see Tab. 2). These high As/Fe values showed a high activity of the partially hydrolyzed iron intercalated in montmorillonites. Among the Fe-Monts, the highest As/Fe molar ratios were obtained for the adsorbents prepared by ion exchange, and the base hydrolysis of excessive iron ions in the montmorillonite mixture (see Tab. 2). From the overall arsenic adsorption results, the 14.0 % Fe-HIPI-Mont was found the best in performance. The isotherms plotted on an iron weight basis also described the high arsenic adsorption

**Table 2.** Saturated arsenic adsorption capacity ( $a$ ), adsorption equilibrium constant ( $K$ ) and the As/Fe molar ratio for the adsorbents used in this study, and comparison with iron oxyhydroxides used in other studies.

Adsorbent	Arsenite			Arsenate		
	$a$ [mg <sub>As</sub> /g <sub>ads</sub> ]	$K$ [mL/g <sub>As</sub> ]	As/Fe [molar ratio]	$a$ [mg <sub>As</sub> /g <sub>ads</sub> ]	$K$ [mL/g <sub>As</sub> ]	As/Fe [molar ratio]
Na-montmorillonite	0	0	0	0	0	0
2.8 % Fe-IE-Mont	1.4	$1.4 \times 10^6$	0.037	4.6	$4.3 \times 10^5$	0.122
14.0 % Fe-HIPI-Mont	8.0	$1.4 \times 10^6$	0.043	75.2	$4.2 \times 10^5$	0.401
15.3 % Fe-IPI-Mont	4.4	$5.1 \times 10^5$	0.021	7.4	$1.4 \times 10^6$	0.036
24.6 % Fe-IPI-Mont	5.3	$5.0 \times 10^5$	0.016	6.1	$2.4 \times 10^6$	0.018
$\alpha$ -FeO(OH)	1.9	$1.4 \times 10^6$	0.002	2.7	$3.2 \times 10^6$	0.003
$\alpha$ -FeO(OH) [6]	13.0	$5.4 \times 10^5$	0.015	13.0	$5.4 \times 10^5$	0.015
$\alpha$ -FeO(OH) [14]	16.6	$5.5 \times 10^5$	0.019	2.0	$1.5 \times 10^5$	0.002

capacities of the Fe-Monts compared to the bulk iron oxyhydroxides (data not shown).

### 3.4 Local Structure of Intercalated Iron and Adsorbed Arsenic Species

The iron species in the Fe-Monts were lacking any long-range order as no characteristic peak of iron oxides appeared in the wide-angle XRD patterns (data not shown). Thus, the local structure of the iron species was studied by XAFS spectroscopy. Fig. 5 presents the iron K-edge  $k^3$  weighted extended X-ray absorption fine structure (EXAFS) function, its associated Fourier transform, and the curve fitting analysis for the 14.0 % Fe-HIPI-Mont. The strongest peak at 1.6 Å in the Fourier transform corresponded to Fe-O. For the next-nearest neighbor, the peak corresponding to Fe...Fe shell appeared at 2.8 Å. The curve fitting results gave a Fe-O bond distance ( $R$ ) of 2.046 Å with a coordination number ( $N$ ) of 6, indicating an octahedral coordination of the intercalated iron species. The results of the curve fitting analysis are given in Tab. 3 and the obtained structural parameters typical of edge-shared octahedral are described in the model structure shown in Fig. 8. The curve fitting results of Fe...Fe shell showed a coordinative unsaturation ( $N$  2.5) of the edge-sharing ( $R$  3.27 Å) iron species as compared to the bulk iron oxyhydroxides ( $N$  6). This unsaturation of the Fe...Fe coordination number in the intercalated iron species was the major reason of their high activity for arsenic removal.

Chemical shifts in the arsenic  $K\alpha_1$  emission spectra were observed for the reference compounds of  $As^{III}O_3$  and  $KH_2As^VO_4$ . In comparison to the arsenic metal  $K\alpha_1$  peak, the chemical shifts of the  $As^{III}O_3$  and  $KH_2As^VO_4$   $K\alpha_1$  peaks were -1.4 and +0.6, respectively. The full width at half maximum (fwhm) for the most symmetrical  $K\alpha_1$  peaks ( $As^{III}$  adsorbed on Fe-montmorillonite) was 3.36 eV (see Fig. 6), whereas the natural core-hole lifetime width of  $K\alpha_1$  was 3.08 eV. Thus, the energy-resolution of this homemade fluorescence spectrometer was estimated to be 1.3 eV, including the contribution of the beamline.

The emission spectra were compared with the reference compounds in order to find out the oxidation state of the arsenic adsorbed on the 14.0 % Fe-HIPI-Mont. The  $K\alpha_1$  emission peak of arsenic adsorbed from the 0.2 to 16 mg/L test solutions of arsenite always appeared at +0.6 eV with reference to arsenic metal. This chemical shift was the same as seen for the arsenic  $K\alpha_1$  peak of  $KH_2As^VO_4$ . The emission spectra are displayed in Fig. 6. The peak position of the  $K\alpha_1$  emission spectrum for the arsenic adsorbed from 16 mg/L of arsenite was observed at 10554.3 eV, similar to that of the arsenate reference compound (10554.9 eV). The starting test solution was of arsenite, but the arsenic  $K\alpha_1$  emission peak showed that the finally adsorbed state was arsenate. This chemical shift indicated an environmentally important phenomenon: the oxidation of the arsenite species to arsenate.

In addition, the comparison of the arsenic K-edge XANES spectra showed that the peak energy positions for the arsenite adsorbed on the intercalated iron species from the

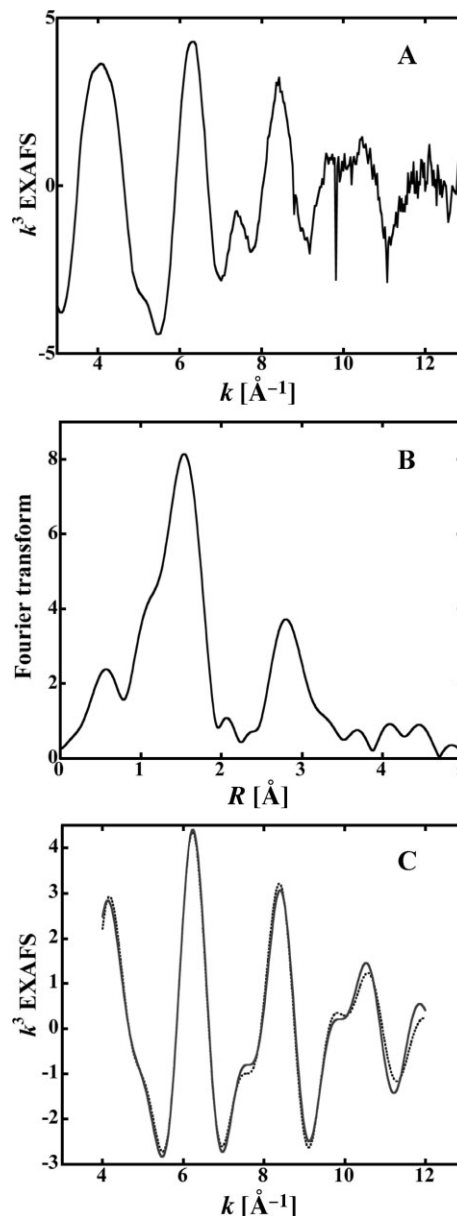


**Figure 5.** (A) Iron K-edge  $k^3$  weighted EXAFS function, (B) its associated Fourier transform and (C) the curve fitting analysis for the 14.0 % Fe-HIPI-Mont. The XAFS spectrum was measured at 290 K. The observed data are shown as a solid line and the fit as a dotted line.

0.2–16 mg/L test solutions were (11871.7–11871.9 eV) close to the value of arsenate (11872.1 eV) rather than the arsenite (11868.6 eV) reference compound (see Fig. 7). No oxidation was reported for the arsenite adsorption from the 6–15 mg/L test solutions on the bulk iron oxyhydroxides [5].

Furthermore, the arsenic K-edge EXAFS curve fitting results for the arsenite adsorbed on iron also confirmed its oxidation (data not shown). For the arsenic adsorbed from the arsenite test solution, the As-O bond distance of 1.68 Å ( $N$  4.2) was

**Table 3.** Iron K-edge EXAFS curve fitting results for the 14.0 % Fe-HIPI-Mont and bulk iron oxyhydroxide.

Sample name	Shell	<i>N</i>	<i>R</i> [Å]	$\Delta E$ [eV]	$\Delta\sigma^2$ [Å <sup>2</sup> ]	Goodness of the fit
Fe-montmorillonite	Fe-O	6.0 (±1.0)	2.046	-0.7	0.0003	256
	Fe•••Fe	2.5 (±0.6)	3.270	-3.1	0.0003	
<i>α</i> -FeO(OH)*	Fe-O	6.0	2.021	n.a.	n.a.	n.a.
	Fe•••Fe	2.0	3.015	n.a.	n.a.	
	Fe•••Fe	6.0	3.390	n.a.	n.a.	

*N*: Coordination number, *R*: Bond distance,  $\Delta E$ : Change in the inner potential,  $\Delta\sigma^2$ : Debye-Waller factor.  
 \* The results are based on the crystallographic data [21].  
 n.a.: not applicable

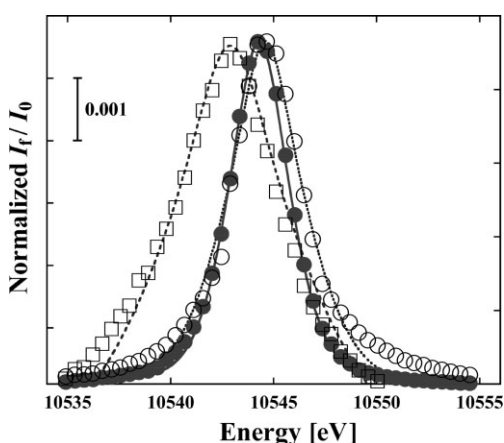


**Figure 6.** Arsenic  $K\alpha_1$  emission spectra for (open squares)  $As_2O_3$ , (open circles)  $KH_2AsO_4$  and arsenic (filled circles) adsorbed on the 14.0 % Fe-HIPI-Mont from the arsenite test solution of 16 mg/L.

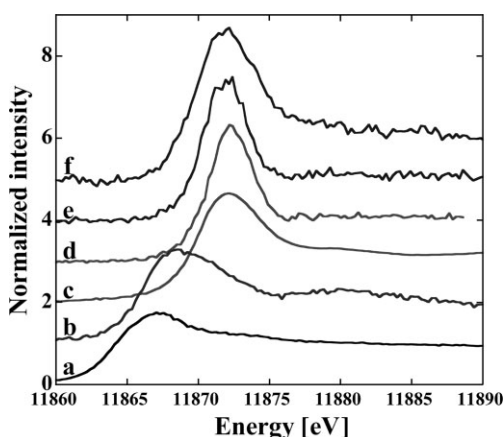


**Figure 7.** The normalized arsenic  $K\alpha_1$ -selecting arsenic K-edge XANES spectra for (a) arsenic metal; (b)  $As_2O_3$ , (c)  $KH_2AsO_4$  and arsenic adsorbed on the 14.0 % Fe-HIPI-Mont from (d) an arsenate test solution of 16 mg/L, (e) an arsenite test solution of 16 mg/L, and (f) an arsenite test solution of 0.2 mg/L.

close to that of arsenate (1.69 Å) rather than arsenite (1.78–1.79 Å) [5, 27]. The As•••Fe *N* value of 2.1 (*R* 3.31 Å) indicated a bidentate binuclear complex formation of oxidized arsenate species with the adjacent apexes of edge-sharing octahedral iron species. The model structure in Fig. 8 describes the mode of the adsorbed arsenic species. XAFS studies also showed that the arsenate species adsorbed on the iron-montmorillonite remained unchanged.

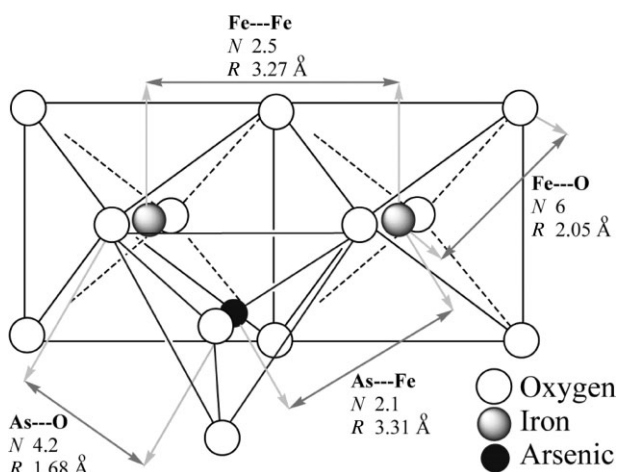


**Figure 8.** Model structure deduced from the X-ray absorption fine structure studies for the edge-sharing octahedral iron species intercalated in montmorillonite and arsenic adsorbed on them.

### 4 Conclusions

Iron-montmorillonites were highly active in arsenic removal. Even though the iron contents of Fe-Monts were low as compared to the bulk iron oxyhydroxides, they were more efficient in arsenic removal. The most active iron species for arsenic adsorption was prepared by ion exchange, and the base hydrolysis of excessive iron ions in the montmorillonite suspension. A high unsaturation of the Fe•••Fe coordination number in the intercalated iron species was an important factor for their high

activity in arsenic adsorption. Along with an efficient arsenic adsorption, the intercalated iron species were effective in the oxidation of arsenite into arsenate.

## Acknowledgements

The authors are highly grateful to the Ministry of Education, Culture, Sports, Science and Technology of the government of Japan for the financial support. The XAFS experiments for arsenic (SPring-8) and iron (KEK-PF) were performed under approvals.

## References

- [1] D. K. Nordstrom, Worldwide occurrences of arsenic in ground water, *Science* **2002**, 296, 2143–2145.
- [2] P. L. Smedley, D. G. Kinniburgh, A review of the source, behavior and distribution of arsenic in natural waters, *Appl. Geochem.* **2002**, 17, 517–568.
- [3] R. S. Oremland, J. F. Stolz, The ecology of arsenic, *Science* **2003**, 300, 939–944.
- [4] A. H. Smith, P. A. Lopipero, M. N. Bates, C. M. Steinmaus, Arsenic epidemiology and drinking water standards, *Science* **2002**, 296, 2145–2146.
- [5] M. L. Farquhar, J. M. Charnock, F. R. Livens, D. J. Vaughan, Mechanisms of arsenic uptake from aqueous solution by interaction with goethite, lepidocrocite, mackinawite, and pyrite: an X-ray absorption spectroscopy study, *Environ. Sci. Technol.* **2002**, 36, 1757–1762.
- [6] S. Dixit, J. G. Hering, Comparison of arsenic(V) and arsenic(III) sorption onto iron oxide minerals: implication for arsenic mobility, *Environ. Sci. Technol.* **2003**, 37, 4182–4189.
- [7] J. A. Wilkie, J. G. Hering, Adsorption of arsenic onto hydrous ferric oxide: effects of adsorbate/adsorbent ratios and co-occurring solutes, *Colloids Surf., A* **1996**, 107, 97–110.
- [8] K. P. Raven, A. Jain, R. H. Leppert, Arsenite and arsenate adsorption on ferrihydrite: kinetics, equilibrium, and adsorption envelopes, *Environ. Sci. Technol.* **1998**, 32, 344–349.
- [9] Y. Izumi, D. Masih, K. Aika, Y. Seida, Creation of micro and mesoporous Fe<sup>III</sup> materials utilizing organic template followed by carboxylates exchange for the low concentrations of arsenite removal, *Micropor. Mesopor. Mater.* **2006**, 94, 243–253.
- [10] M. Bissen, F. H. Frimmel, Arsenic – a review, Part II: Oxidation of arsenic and its removal in water treatment, *Acta Hydrochim. Hydrobiol.* **2003**, 31, 97–107.
- [11] S. Buddhawong, P. Kusch, J. Mattusch, A. Wiessner, U. Stottmeister, Removal of arsenic and zinc using different laboratory model wetland systems, *Eng. Life Sci.* **2005**, 5 (3), 247–252. DOI: 10.1002/elsc.200520076
- [12] J. M. Thomas, Sheet silicate intercalates: new agents for unusual chemical conversions, in *Intercalation Chemistry* (Eds: M. S. Whittingham, A. J. Jacobson), Academic Press, New York **1982**, 55–99.
- [13] S. Yamanaka, T. Doi, S. Sako, M. Hattori, High surface area solids obtained by intercalation of iron oxide pillars in montmorillonite, *Mat. Res. Bull.* **1984**, 19, 161–168.
- [14] V. Lenoble, O. Bouras, V. Deluchat, B. Serpaud, J. C. Bollinger, Arsenic adsorption onto pillared clays and iron oxides, *J. Colloid Interface Sci.* **2002**, 255, 52–58.
- [15] J. Q. Jiang, C. Cooper, S. Ouki, Comparison of modified montmorillonite adsorbents, Part I: Preparation, characterization and phenol adsorption, *Chemosphere* **2002**, 47, 711–716.
- [16] D. C. Koningsberger, R. Prins, *X-Ray Absorption – Principles, Applications, Techniques of EXAFS, SEXAFS and XANES*, John Wiley & Sons, New York **1988**.
- [17] Y. Izumi, D. Masih, K. Aika, Y. Seida, Characterization of intercalated iron(III) nanoparticles and oxidative adsorption of arsenite on them monitored by X-ray absorption fine structure combined with fluorescence spectrometry, *J. Phys. Chem. B* **2005**, 109, 3227–3232.
- [18] Y. Izumi, F. Kiyotaki, T. Minato, Y. Seida, X-Ray absorption fine structure combined with fluorescence spectrometry for monitoring trace amounts of lead adsorption in the environmental conditions, *Anal. Chem.* **2002**, 74, 3819–3823.
- [19] J. A. Bearden, X-ray wavelengths, *Rev. Mod. Phys.* **1967**, 39, 78–124.
- [20] R. L. Blake, R. E. Hessevick, T. Zoltani, L. W. Finger, Refinement of the hematite structure, *Am. Mineral.* **1966**, 51, 123–129.
- [21] G. A. Waychunas, C. C. Fuller, B. A. Rea, J. A. Davis, Wide angle X-ray scattering (WAXS) study of “two-line” ferrihydrite structure: Effect of arsenate sorption and counterion variation and comparison with EXAFS results, *Geochim. Cosmochim. Acta* **1996**, 60, 1765–1781.
- [22] K. Ebitani, M. Ide, T. Mitsudome, T. Mizugaki, K. Kaneda, Creation of a chain-like cationic iron species in montmorillonite as a highly active heterogeneous catalyst for alkane oxygenations using hydrogen peroxide, *Chem. Commun.* **2002**, 690–691.
- [23] J. M. Brendle, L. Khouchaf, J. Baron, R. L. Dred, M.-H. Tullier, Zr-exchanged and pillared beidellite: preparation and characterization by chemical analysis, XRD and Zr K EXAFS, *Microporous Mater.* **1997**, 11, 171–183.
- [24] R. E. Grim, *Clay Mineralogy*, 2nd ed., McGraw-Hill, New York **1968**.
- [25] F. Rouquerol, J. Rouquerol, K. Sing, *Adsorption by Powders and Porous Solids – Principles, Methodology and Applications*, Academic Press, London **1999**.
- [26] B. A. Manning, S. Goldberg, Modeling arsenate competitive adsorption on kaolinite, montmorillonite and illite, *Clays Clay Miner.* **1996**, 44, 609–623.
- [27] B. A. Manning, S. E. Fendorf, S. Goldberg, Surface structures and stability of arsenic(III) on goethite: spectroscopic evidence for inner-sphere complexes, *Environ. Sci. Technol.* **1998**, 32, 2383–2388.